

*This is the peer reviewed version of the following article: Urošević, A., Ajduković, M., Vučić, T., Scholtes, S.J., Arntzen J.W., Ivanović, A. (2023). Regionalization and morphological integration in the vertebral column of Eurasian small-bodied newts (Salamandridae: *Lissotriton*). Journal of Experimental Zoology Part B – Molecular and Developmental Evolution, which has been published in final form at <http://doi.org/10.1002/jez.b.23205> .*

This article may be used for non-commercial purposes in accordance with Wiley Terms and Conditions for Use of Self-Archived Versions. This article may not be enhanced, enriched or otherwise transformed into a derivative work, without express permission from Wiley or by statutory rights under applicable legislation.

Copyright notices must not be removed, obscured or modified. The article must be linked to Wiley's version of record on Wiley Online Library and any embedding, framing or otherwise making available the article or pages thereof by third parties from platforms, services and websites other than Wiley Online Library must be prohibited.

1 **Regionalization and morphological integration in the vertebral column of Eurasian small-**
2 **bodied newts (Salamandridae: *Lissotriton*)**

3
4 Aleksandar Urošević^{1,*}, Maja Ajduković¹, Tijana Vučić^{2,3,4}, Stefan J. Scholtes⁴, Jan W.
5 Arntzen^{3,4}, Ana Ivanović²

6
7 ¹Department of Evolutionary Biology, Institute for Biological Research "Siniša Stanković",
8 National Institute of the Republic of Serbia, University of Belgrade, Belgrade, Serbia

9 (aurosevic@ibiss.bg.ac.rs, <https://orcid.org/0000-0003-1158-5537>;

10 maja.ajdukovic@ibiss.bg.ac.rs, <https://orcid.org/0000-0001-9115-6622>)

11 ²Faculty of Biology, University of Belgrade, Belgrade, Serbia (ana@bio.bg.ac.rs,

12 <https://orcid.org/0000-0002-6247-8849>)

13 ³Institute of Biology, Leiden University, Leiden, The Netherlands

14 (t.vucic@biology.leidenuniv.nl, <https://orcid.org/0000-0002-8850-5251>)

15 ⁴Naturalis Biodiversity Center, Leiden, The Netherland (stefan.scholtes16@gmail.com,

16 <https://orcid.org/0000-0001-9320-4296>; pim.arntzen@naturalis.nl, [https://orcid.org/0000-0003-](https://orcid.org/0000-0003-3229-5993)
17 [3229-5993](https://orcid.org/0000-0003-3229-5993))

18

19 **Data availability statement:** The raw shape coordinates, size values (centroid size) and R
20 scripts underlying this article are publicly available as Supplementary information to the
21 published version of the article.

22 **Funding statement:** This work was funded by the Serbian Ministry of Education, Science and
23 Technological Development grants numbers 451-03-68/2022-14/ 200007 and 451-03-68/2022-
24 14/200178

25 **Conflict of interest disclosure:** The authors declare no conflicts of interest.

26 **Ethics approval statement:** N/A

27 **Patient consent statement:** N/A

28 **Permission to reproduce material from other sources:** N/A

29 **Clinical trial registration:** N/A

30

31

32

33

34

35

36

37

38

39

40

41

42

43 **Abstract**

44 Serially homologous structures may have complex patterns of regionalization and morphological
45 integration, influenced by developmental *Hox* gene expression and functional constraints. The
46 vertebral column, consisting of a number of repeated, developmentally constrained and highly
47 integrated units – vertebrae – is such a complex serially homologous structure. Functional
48 diversification increases regionalization and modularity of the vertebral column, particularly in
49 mammals. For salamanders, three concepts of regionalization of the vertebral column have been
50 proposed, recognizing one, two or three presacral regions. Using 3D geometric morphometrics
51 on vertebra models acquired with micro-CT scanning we explored the covariation of vertebrae in
52 four closely related taxa of small-bodied newts in the genus *Lissotriton*. The data were analyzed
53 by segmented linear regression to explore patterns of vertebral regionalization and by a two-
54 block partial least squares method to test for morphological integration. All taxa show a
55 morphological shift posterior to the 5th trunk vertebra, which corresponds to the two-region
56 concept. However, morphological integration is found to be strongest in the mid-trunk. Taken
57 jointly, these results indicate highly integrated presacral vertebral column with a subtle two-
58 region differentiation. The results are discussed in relation to specific functional requirements,
59 developmental and phylogenetic constraints, and specific requirements posed by a biphasic life
60 cycle and different locomotor modes (swimming vs. walking). Further research should be
61 conducted on different ontogenetic stages and closely related but ecologically differentiated
62 species.

63

64 **Keywords:** axial skeleton, geometric morphometrics, micro-CT scanning, modularity, regional
65 differentiation, serial homology, tailed amphibians

66 **Introduction**

67 Morphological integration is defined as the covariation of morphological traits as a result of
68 developmental and functional interactions (Olson & Miller, 1958), but may also be shaped by
69 selective pressures (Cheverud, 1996; Wagner & Altenberg, 1996; Klingenberg, 2008; Zelditch &
70 Goswami, 2021). Modularity implies variation in integration within an organism and some parts
71 can be more integrated than others. Accordingly, morphological modules are interpreted as units
72 with strong covariation within and minor covariation among units.

73 Serially homologous structures such as vertebrae, teeth and ribs provide worthwhile
74 model systems for the study of regionalization, modularity and morphological integration,
75 because they share a common structural plan with variation throughout the series (Gómez-Robles
76 & Polly, 2012; Jones et al., 2018; Urošević et al., 2020). Elements within serially homologous
77 structures tend to be developmentally constrained and strongly integrated (Cowley & Atchley,
78 1990; Carroll, 2001; Young & Hallgrímsson, 2005; Asher et al., 2011; Jones et al., 2018, 2020).
79 In some cases, different functional demands and selection pressures may lead to the
80 “parcellation” of regional differentiation (Wagner & Altenberg, 1996), such as in the limb
81 skeleton (Young & Hallgrímsson, 2005), the feeding apparatus (Wainwright, 2007) and the
82 vertebral column (Randau & Goswami, 2017; Jones et al., 2020). For example, the mammalian
83 presacral vertebral column is markedly regionalized and can be divided into several
84 developmental and functional modules (Randau & Goswami, 2017).

85 The evolution of vertebral modularity appears largely driven by locomotion and ecology
86 (Galis et al., 2014; Jones et al., 2018) and is also under developmental constraints (Galis, 1999).
87 The vertebral column can be viewed as an integrated structure because it derives entirely from
88 the somites (the presomitic mesoderm) and it has independent developmental and evolutionary

89 patterns derived from the abaxial domain of the mesoderm (Shearman & Burke, 2009). The
90 shape of vertebrae and regionalization of the vertebral column are determined throughout the
91 early ontogenetic stages by spatial and temporal expression of the *Hox* genes during
92 somitogenesis (Krumlauf, 1994; Aulehla & Pourguié, 2010; Mallo et al., 2010). The boundaries
93 in *Hox* genes expression correspond to the boundaries of the vertebral regions. In mammals, the
94 expression boundary of the *Hox6* gene determines the cervico-thoracic transition, *Hox10* the
95 thoraco-lumbar and *Hox11* the lumbar-sacral transition (Burke et al., 1995; Wellik, 2007;
96 Kuratani, 2009). This tetrapod-like organization of *Hox* genes expression has presumably a deep
97 evolutionary origin and may have arisen in the first jawed vertebrates (Criswell et al., 2021).
98 Some well-preserved fossil skeletons of the early tetrapod *Ichthyostega* had recognizable
99 thoracic, lumbar, sacral and caudal vertebral regions (Ahlberg et al., 2005), suggesting that the
100 regionalization of the vertebral column was, be it only subtly expressed, present in the stem
101 tetrapod lineage (Head & Polly, 2015; Jones et al., 2018).

102 In extant amphibians the vertebral column encompasses three distinctive body plans as
103 found in the tailless frogs and toads (Anura), the elongated, limbless caecilians (Gymnophiona)
104 and the tailed amphibians or salamanders (Caudata). Salamanders have a cylindrical body with a
105 poorly differentiated vertebral column, four relatively short appendages and a tail (Mivart, 1870;
106 Duellman & Trueb, 1994). They have widely been used as morphological analogues to the early
107 terrestrial vertebrates that presumably possessed the same general body plan and similar modes
108 of locomotion. Their presacral vertebral column consists of a single cervical vertebra (the atlas)
109 which articulates to the skull and lack ribs, and a series of rib-bearing trunk vertebrae. They also
110 have a single sacral vertebra, several postsacral and numerous caudal vertebrae, depending on
111 the species (Duellman & Trueb, 1994; Litvinchuk & Borkin, 2003; Lanza et al., 2010) (Fig. 1A).

112 Recent studies on vertebral regionalization (Jones et al., 2018) and morphological differentiation
113 (Scholtes et al., 2021) indicate that the trunk region in salamanders is not as uniform as
114 previously thought. A three-region pattern of the presacral vertebral column was found in
115 *Ambystoma* (Jones et al., 2018). In small-bodied newts of the genus *Lissotriton* substantial
116 morphological differentiation in the vertebrae shape along the trunk region was documented (Fig
117 1A; Scholtes et al., 2021). We here provide a brief description of three alternative concepts of the
118 salamander's presacral vertebral column regionalization (see Table 1).

119 The vertebral column of tailed amphibians has traditionally been regarded as not, or
120 poorly differentiated (Mivart, 1870; Duelman & Trueb, 1994, Slijepčević et al., 2015). The
121 presacral vertebral column was in its entirety (minus the atlas) designated as the 'trunk region',
122 due to a shared gross morphology of rib-bearing vertebrae. Subsequently Jones et al. (2018),
123 using *Ambystoma* as model species, proposed a three-region differentiation of the salamander
124 presacral vertebral column. The first region associates with the posterior branch of the brachial
125 plexus, implying homology of the anterior trunk vertebrae with the cervical region, whereas the
126 middle and posterior region correspond to regions of short and long ribs in the Amniotes (Jones
127 et al., 2018). Alternatively, studies on morphometric variation in vertebrae size (Worthington &
128 Wake, 1972; Govedarica et al., 2017) and shape (Scholtes et al., 2021) revealed morphological
129 differentiation (substantial disparity in size and shape) of the presacral vertebral column in
130 salamanders, particularly in the anterior trunk vertebrae. A similar heterogeneity among short
131 and bulky anterior and elongated posterior vertebrae was documented in caecilians (Lowie et al.,
132 2022). The morphological differentiation and disparity of anterior trunk vertebrae have been
133 explained by different functional demands upon anterior vertebrae compared to the subsequent,
134 posterior ones (Worthington & Wake, 1972; Scholtes et al., 2021).

135 We gathered data on *Lissotriton* vertebrae size and shape to analyze patterns of
136 covariation (allometric variation, regionalization and integration), and we discuss our findings
137 relative to three concepts of differentiation of the vertebral column in salamanders. Allometric
138 variation is analysed because it is generated by variation in developmental processes that affect
139 multiple traits, resulting in overall patterns of covariation, and it contributes to morphological
140 integration and modularity (Mitteroecker & Bookstein, 2007; Klingenberg, 2013, 2016;
141 Hallgrímsson et al., 2019). To explore regionalization, we used segmented linear regression
142 (SLR) (Head & Polly, 2015; Jones et al., 2018) which provides information on the most probable
143 changes in the pattern of covariation and suggests possible regions. Morphological integration
144 was quantified as the strength of covariation among vertebrae using two-block partial least
145 squares (PLS) (e.g., Bastir & Rosas, 2005; Klingenberg, 2009). We expected to observe higher
146 integration within regions and lower integration among vertebrae from different regions.

147

148 **Material and Methods**

149 The studied material consists of 74 adult male specimens belonging to two closely related
150 species *Lissotriton schmidtleri* (Raxworthy, 1988) and *L. vulgaris*, the latter being represented by
151 the subspecies *L. v. vulgaris* (Linnaeus, 1758), *L. v. ampelensis* (Fuhn, 1951) and *L. v.*
152 *meridionalis* (Boulenger, 1882). These taxa were chosen because they are phylogenetically close
153 (Pabijan et al., 2017) and show similar patterns of morphological differentiation of the trunk
154 region (Scholtes et al., 2021).

155 The material was either ethanol preserved as is, or prepared as cleared and stained
156 skeletons preserved in glycerin. Detailed sample data on taxonomy, geographical origin, type of
157 preservation and collection details are provided in Appendix I. For each specimen the atlas, the

158 1st to 12th or 13th trunk vertebrae and the sacral vertebrae were scanned with a SkyScan 1172
159 micro-CT scanner (Bruker Corporation) at a resolution of 26.33 μM (32 kV, 0.5 μM aluminium
160 filter, 0.7 degrees rotation steps, 175 ms exposure time, 180 degrees object scanning and a
161 manual flat field correction set at 35 kV). The data were processed into 3D models with Avizo
162 9.5 software (FEI, Thermo Fisher Scientific) (Figure 1A). The configurations of 14 landmarks
163 for the atlas and 18 landmarks for the trunk and sacral vertebrae (Figure 1B) were digitized using
164 the Landmark IDAV 141 v.3.6 software (<https://landmark2.software.informer.com/3.6/>) by a
165 single observer (MA). A morphological description of the landmarks is provided in Appendix II.
166 Raw morphometric data is provided in a supplementary file (Supplementary data S1).

167

168 *Shape variables*

169 We generated the matrix of shape coordinates for each vertebra using a generalized Procrustes
170 analysis (GPA) (Rohlf & Slice, 1990; Dryden & Mardia, 1998), that accounts for object
171 symmetry and quantifies the symmetric components of shape variation (Klingenberg et al.,
172 2002). The principal components (PC scores) from principal component analysis were used as
173 shape variables and centroid size (CS) was used as a measure of general size (Zelditch et al.,
174 2012). CS values are provided in a supplementary file (Supplementary data S1). For the subset of
175 individuals ($N = 12$, 7 *L. v. meridionalis* and 5 *L. v. vulgaris*) for which standard length (Snout-
176 vent length, SVL) was available, we found a strong correlation between CS and standard body
177 length ($r = 0.88$, $p < 0.05$ and $r = 0.99$, $p < 0.05$, respectively).

178

179 *Analyses of allometric variation*

180 For each vertebra the divergence in allometric slopes among taxa was tested for homogeneity of
181 regression slopes with a multivariate analysis of covariance (MANCOVA), with shape variables
182 (PC scores) as the dependent variables, (sub)species as a factor and log-transformed CS (logCS)
183 as a covariate. For the comparisons of allometric variation among vertebrae within the vertebral
184 column, the subset of *T. v. vulgaris* with the largest sample size (n = 47, Appendix I) was used.
185 The homogeneity of slopes was similarly tested with vertebra as a factor. The differences in
186 allometric slopes between vertebrae were further explored by comparisons of allometric
187 regression slopes among vertebrae. At statistical evaluation the Bonferroni correction for
188 multiple comparisons was applied. The PCAs were done with MorphoJ software v. 1.06
189 (Klingenberg, 2011) and MANCOVAs were done with the Statistica 10 software package
190 (Statistica for Windows; StatSoft, Inc., Tulsa, USA).

191

192 *Trunk regionalization*

193 Principal component analysis on the mean shape values of the individual trunk vertebrae for each
194 (sub)species was used to explore patterns of shape variation and for SLR analyses. The series of
195 continuous regression lines was fit to the slopes of the PC scores, and boundaries of regions were
196 determined from the transition points that minimized the sum of squares (Head & Polly, 2015).
197 The Akaike information criterion (AIC) weighted average of the relative fit was calculated to
198 represent the amount of regionalization for each of the region models (Jones et al., 2018) with a
199 maximum of three, for the cervical, thoracic and lumbar region. The SLR- and AIC-fittings were
200 calculated with the *Regions* package (Jones, 2018) in R version 4.1.1. (R core team, 2021).

201

202 *Morphological integration*

203 To estimate the strength of covariation between vertebrae we employed a two-block PLS
204 analysis, based on a singular value decomposition of the matrix of covariances between the two
205 sets of variables (Bookstein, 1991; Rohlf & Corti, 2000; Young & Hallgrímsson, 2005). This
206 approach is suitable for testing covariation between the two separate sets of landmarks, with
207 separate Procrustes superimpositions (Bastir & Rosas, 2005; Klingenberg, 2009; McCane &
208 Kean, 2011; Neaux et al., 2013; Urošević et al., 2020). The measures of covariation between the
209 vertebrae were the RV coefficient (Klingenberg, 2009, 2011) and z-scores (Adams & Collyer,
210 2016). The RV coefficient is a generalization of Pearson's correlation coefficient (Escoufier,
211 1973). Statistical significance of the RV coefficients was assessed via a permutation test against
212 a null hypothesis of total independence (Good, 2000; Manly, 2007; Klingenberg, 2009, 2011)
213 under Bonferroni correction for multiple comparisons. Because the use of the RV coefficient has
214 been criticized on the ground that it is sensitive to sample size and other variables (Adams, 2016;
215 Adams & Collyer, 2016) we repeated analyses corrected for the effect of (sub)species by
216 applying multivariate regression, with shape as the dependent variable and (sub)species
217 numerically coded and used as an independent variable. Two-block PLS was then done on the
218 regression residuals. For the quantification of the covariation strength we used z-scores, centered
219 on their estimated empirically expected values, with statistical significance estimated by a
220 randomization test with 999 permutations (Adams & Collyer, 2016).

221 Morphological integration was tested between structures (atlas, trunk and sacral
222 vertebrae) in pairwise manner on the covariance matrices pooled within taxa. RV coefficients
223 were calculated with MorphoJ software v. 1.06 (Klingenberg, 2011) and z-scores were calculated
224 with *Geomorph 4.0.0.* package (Adams et al., 2021). A heat map visualization of the results was

225 produced with the *Lattice* and *LatticeExtra* packages (Sarkar, 2008; Sarkar & Andrews, 2019) in
226 R. All R scripts used are provided as a supplementary file (Supplementary data S2).

227

228 **Results**

229 *Analyses of allometric variation*

230 The MANCOVA analysis testing for homogeneity of allometric slopes between sub(species)
231 over individual vertebrae (Supplementary Table S3) showed that allometry was not statistically
232 significant, except for the 10th and 11th trunk vertebrae ($F_{26,42} = 2.85$, $P = 0.0012$ and $F_{26,39} =$
233 3.06 , $P = 0.0008$, respectively). A significant (sub)species \times logCS interaction ($F_{78,117.49} = 1.87$, P
234 $= 0.001$) was found only for the 7th trunk vertebra which also diverged in shape among taxa
235 ($F_{78,117.49} = 1.81$, $P = 0.002$).

236 A statistically significant difference of allometric slopes of vertebrae was found within
237 the vertebral column (Table 2). Pairwise comparisons revealed highly significant slope
238 differences between the 3th and 5th and 6th and 12th trunk vertebrae (Table 3). Because of the
239 absence of statistically significant allometry at the sub(species) level and statistically significant
240 differences in allometric slopes between vertebrae along the vertebral column, we did not apply a
241 correction for allometry in subsequent analyses.

242

243 *Trunk regionalization*

244 Similar patterns of variation in vertebrae shape were found across the four (sub)species (Figure
245 2). In all taxa the first and second PC axes together explained >90% of the total shape variation.
246 The first axis explained a shape gradient from the shortened and widened anterior vertebrae with
247 increased height to the elongated, narrower posterior vertebrae with reduced height. The second

248 axis explained a shift from the mid-trunk vertebrae which were shorter, with a higher neural arch
249 to the posterior-most vertebrae that were elongated, with a reduced neural arch (Figure 2). The
250 SLR analyses yielded the best fit for the two-region model (Table 1). The transition point
251 corresponded to the 5th trunk vertebra in all taxa (Table 4, Figure 3).

252

253 *Morphological integration*

254 The estimation of morphological integration ranged from moderate ($0.3 < RV < 0.5$) to strong
255 ($RV > 0.5$) and was statistically significant for all pairs of vertebrae, except for the atlas and all
256 other vertebrae, excluding the 1st, 2nd and 5th trunk vertebrae. The strongest morphological
257 integration was detected at the 6th and 7th trunk vertebrae (Figure 4; Supplementary table S2).
258 Integration levels estimated from z-scores varies from weak ($z < 2$) to moderate ($2 < z < 4$) and
259 strong ($z > 4$) and was the highest between the 3rd and 7th trunk vertebrae. The strongest
260 integration between adjacent vertebrae was between the 1st and 2nd, 2nd and 3rd, 5th and 6th and 8th
261 and 9th trunk vertebrae. Among the adjacent trunk vertebrae, there was no significant integration
262 between the 9th and 10th and the 11th and 12th (Figure 4, Supplementary table S4).

263

264 **Discussion**

265 The tetrapod body plan is determined by *Hox* genes and is largely developmentally constrained.
266 The regionalization of the vertebral column in tetrapods, which is most pronounced in mammals,
267 is largely driven by various functional demands (Carroll, 1997; Jones et al., 2018). Based on
268 morphological, developmental and functional criteria and the literature we considered three
269 concepts of vertebral column regionalization in salamanders, in which one, two or three presacral
270 regions are recognized (Table 1). Considering the results for both analytical methods separately,

271 our data support the traditional concept of regionalization with a single, highly integrated trunk,
272 and the two regions concept, which recognizes an anterior and a posterior trunk region.

273 The results are not unequivocal because the differentiation into an anterior and a posterior
274 region with a break between the 5th and 6th trunk vertebrae recognized by the SLR analysis is not
275 supported by the pattern of morphological integration observed by the PLS analysis. The
276 vertebrae within regions should, by definition, be more integrated than between regions (Wagner
277 & Altenberg, 1996; Klingenberg, 2008). However, the morphological integration is found to be
278 strongest in the mid-trunk (Figure 4) where the break point between the regions is detected
279 (Figure 3). The strong individual integration between the adjacent 1st, 2nd and 3rd vertebrae could
280 be related to the center of the anterior region whereas the atlas, sacral vertebra and 12th trunk
281 vertebra tend to have some autonomy from the remaining trunk vertebrae.

282 In summary, our results suggest a subtle pattern of regionalization, corresponding to a
283 functionally-based, two-region concept, despite a high level of integration that was observed in
284 the anterior and middle parts of the presacral vertebral column. The marked morphological
285 integration could be explained by the homogeneity of the whole vertebral column as possibly
286 required for its functional stability (Arlegi et al., 2020). In salamanders the vertebral column,
287 together with the axial musculature, provides support and locomotion in aquatic as well as
288 terrestrial environments (Duellman & Trueb, 1994). The axial musculoskeletal system in
289 salamanders has been described in detail for the fire salamander, *Salamandra salamandra*
290 (Linnaeus, 1758) (Francis, 1934). The dorsal musculature arrangement is more or less uniform,
291 with a main function in the bending and flexion of the spine. The first to fifth trunk vertebrae are
292 involved in movements of the pectoral girdle and the front limbs. The first and second trunk
293 vertebrae are connected with the cranial skeleton with the muscles involved in the coordinated

294 head movement and spine flexion (Francis, 1934). This could explain the covariation between
295 the 1st to 5th trunk vertebrae, notwithstanding their differences in shape (Scholtes et al., 2021).
296 The posterior region (from the 6th to the 11th or the 12th vertebra) consists of vertebrae with
297 similar shape and the same arrangement of muscles driving the lateral bending of the trunk
298 during swimming and walking.

299 In salamanders, the axial skeleton forms during early development and remains largely
300 unchanged during the metamorphosis. It has been proposed that the complex life cycle, with
301 opposing functional requirements upon the axial skeleton during the larval and adult phases,
302 constrain evolutionary changes in the vertebral column (Bonett & Blair, 2017). Therefore,
303 changes in the pattern of regionalization might be expected in non-metamorphic taxa, including
304 paedomorphic lineages (e.g., Sirenidae, Proteidae) and in lineages with direct development
305 (Plethodontidae). However, a different regionalization pattern was found in *Ambystoma* with
306 three regions (Jones et al., 2018) and *Lissotriton* with two regions (this study), that both have a
307 complex life cycle and similar requirements for locomotory performance (swimming vs.
308 walking). Compared to the three-region hypothesis of differentiation described for *Ambystoma*
309 (Jones et al., 2018), the anterior trunk region in *Lissotriton* coincides with the “cervical” region
310 whereas the posterior trunk region is uniform, without detectable differentiation in the
311 subsequent anterior and posterior “dorsal” region (Jones et al., 2018). As clades *Ambystoma* and
312 *Lissotriton* are unrelated. It is possible that *Ambystoma* kept the ancestral condition of
313 regionalization including an ancestral amphicoelous morphology of the vertebrae, compared to
314 the derived condition of ophisthocoelous vertebrae found in the family Salamandridae
315 (Worthington & Wake, 1972; Duelman & Trueb, 1994). The morphometric study of
316 Worthington & Wake (1972) also found that species belonging to different lineages of tailed

317 amphibians (namely Ambystomatidae, Salamandridae and Plethodontidae) have different
318 patterns of morphometric variation along the vertebral column.

319 To further explore patterns of vertebral regionalization, modularity and morphological
320 integration in salamanders, it would be beneficial to include different life stages (e.g., larvae vs.
321 metamorphs), or closely related, but ecologically differentiated forms. For the genus *Lissotriton*,
322 this points to paedomorphic populations such as found in *L. vulgaris* (Toli et al., 2022) and to the
323 frequently stream-dwelling *L. boscai* (Lataste, 1879) from the Iberian Peninsula. Related species
324 with different numbers of presacral vertebrae such as found within the genera *Triturus* and
325 *Tylotriton* warrant attention (Arntzen et al., 2015), as does the genus *Salamandra* for which
326 larviparous, pueriparous and viviparous lineages can be compared (Buckley et al., 2007). Ideally,
327 these studies would be accompanied by data on *Hox* gene expression.

328

329 **Acknowledgements**

330 We thank Katrina E. Jones for help and advice with the *Regions* package. We also thank two
331 anonymous reviewers for critical comments and suggestions that helped to improve the
332 manuscript. Our work was funded by the Serbian Ministry of Education, Science and
333 Technological Development grants numbers 451-03-68/2022-14/ 200007 and 451-03-68/2022-
334 14/200178.

335

336 **References**

337 Adams, D.C. (2016). Evaluating modularity in morphometric data: challenges with the RV
338 coefficient and a new test measure. *Methods in Ecology and Evolution*, 7, 565–572.
339 <https://doi.org/10.1111/2041-210X.12511>

340 Adams, D.C., & Collyer, M.L. (2016). On the comparison of the strength of morphological
341 integration across morphometric datasets. *Evolution*, 70, 2623–2631.
342 <https://doi.org/10.1111/evo.13045>

343 Adams, D.C., Collyer, M.L., Kaliontzopoulou, A., & Baken, E. (2021). Geomorph. Geometric
344 Morphometric Analyses of 2D/3D Landmark Data. R package.
345 <https://github.com/geomorphR/geomorph>

346 Ahlberg, P.E., Clack, J.A., & Blom, H. (2005). The axial skeleton of the Devonian tetrapod
347 *Ichthyostega*. *Nature*, 437, 137–140. <https://doi.org/10.1038/nature03893>

348 Arlegi, M., Veschambre-Couture, C., & Gómez-Olivencia, A. (2020). Evolutionary selection and
349 morphological integration in the vertebral column of modern humans. *American Journal*
350 *of Physical Anthropology*, 171, 17–36. <https://doi.org/10.1002/ajpa.23950>

351 Arntzen, J.W., Beukema, W., Galis, F., & Ivanović, A. (2015). Vertebral number is highly
352 evolvable in salamanders and newts (family Salamandridae) and variably associated with
353 climatic parameters. *Contributions to Zoology*, 84, 85–113.
354 <https://doi.org/10.1163/18759866-08402001>

355 Asher, R., Lin, K., Kardjilov, N., & Hautier, L. (2011). Variability and constraint in the
356 mammalian vertebral column. *Journal of Evolutionary Biology*, 24, 1080–1090.
357 <https://doi.org/10.1111/j.1420-9101.2011.02240.x>

358 Aulehla, A., & Pourguié, O. (2010). Signaling gradients during paraxial mesoderm development.
359 *Cold Spring Harbor Perspectives in Biology*, 2, a000869.
360 <https://doi.org/10.1101/cshperspect.a000869>.

361 Bastir, M., & Rosas, A. (2005). Hierarchical nature of morphological integration and modularity
362 in the human posterior face. *American Journal of Physical Anthropology*, 128, 26–34.
363 <https://doi.org/10.1101/10.1002/ajpa.20191>

364 Bonett, R.M., & Blair, A.L. (2017). Evidence for complex life cycle constraints on salamander
365 body form diversification. *Proceedings of the National Academy of Sciences*, 114, 9936–
366 9941. <https://doi.org/10.1073/pnas.1703877114>

367 Bookstein, F.L. (1991). Morphometric tools for landmark data: geometry and biology.
368 Cambridge: Cambridge University Press.

369 Burke, A.C., Nelson, C.E., Morgan, B.A., & Tabin, C. (1995). *Hox* genes and the evolution of
370 vertebrate axial morphology. *Development*, 121, 333–346.
371 <https://doi.org/10.1242/dev.121.2.333>

372 Buckley, D., Alcobendas, M., García-París, M., & Wake, M.H. (2007). Heterochrony,
373 cannibalism, and the evolution of viviparity in *Salamandra salamandra*. *Evolution and*
374 *Development*, 9, 105–115. <https://doi.org/10.1111/j.1525-142X.2006.00141.x>

375 Carroll, R.L. (1997). Patterns and processes of vertebrate evolution. Cambridge: Cambridge
376 University Press.

377 Carroll, S.B. (2001). Chance and necessity: the evolution of morphological complexity and
378 diversity. *Nature*, 409, 1102–1109. <https://doi.org/10.1038/35059227>

379 Cheverud, J.M. (1996). Developmental integration and the evolution of pleiotropy. *American*
380 *Zoologist*, 36, 44–50.

381 Cowley, D.E., & Atchley, W.R. (1990). Development and quantitative genetics of correlation
382 structure among body parts of *Drosophila melanogaster*. *The American Naturalist*, 135,
383 242–268. <https://doi.org/10.1086/285041>

384 Criswell, K.E., Roberts, L.E., Koo, E.T., Head, J.J., & Gillis, J.A. (2021). *Hox* gene expression
385 predicts tetrapod-like axial regionalization in the skate, *Leucoraja erinacea*. *Proceedings*
386 *of the National Academy of Sciences*, 118, e2114563118.
387 <https://doi.org/10.1073/pnas.2114563118>

388 Dryden, I.L., & Mardia, K.V. (1998). *Statistical Shape Analysis*. New York: Wiley.

389 Duellman, W.E., & Trueb, L. (1994). *Biology of Amphibians*. Maryland: Johns Hopkins
390 University Press.

391 Escoufier, Y. (1973). Le traitement des variables vectorielles. *Biometrics*, 29, 751–760.
392 <https://doi.org/10.2307/2529140>

393 Francis, E.B.T. (1934). *The anatomy of the salamander*. Oxford: Clarendon Press.

394 Galis, F. (1999). Why do almost all mammals have seven cervical vertebrae? Developmental
395 constraints, *Hox* genes and cancer. *Journal of Experimental Zoology Part B: Molecular*
396 *and Developmental Evolution*, 285, 19–26.

397 Galis, F., Carrier, D.R., van Alphen, J., van der Mije, S.D., Van Dooren, T.J., Metz, J.A., & ten
398 Broek, C.M. (2014). Fast running restricts evolutionary change of the vertebral column in
399 mammals. *Proceedings of the National Academy of Sciences*, 111, 11401–11406.
400 <https://doi.org/10.1073/pnas.1401392111>

401 Gómez-Robles, A., & Polly, D.P. (2012). Morphological integration in the hominin dentition:
402 Evolutionary, developmental, and functional factors. *Evolution*, 66, 1024–1043.
403 <https://doi.org/10.1111/j.1558-5646.2011.01508.x>

404 Good, P. (2000). *Permutation tests: a practical guide to resampling methods for testing*
405 *hypotheses* (2nd ed.). New York: Springer.

406 Govedarica, P., Cvijanović, M., Slijepčević, M., & Ivanović, A. (2017). Trunk elongation and
407 ontogenetic changes in the axial skeleton of *Triturus* newts. *Journal of Morphology*, 278,
408 1577–1585. <https://doi.org/10.1002/jmor.20733>

409 Hallgrímsson, B., Katz, D.C., Aponte, J.D., Larson, J.R., Devine, J., Gonzalez, P.N., Young,
410 N.M., Roseman, C.C., & Marcucio, R.S. (2019). Integration and the Developmental
411 Genetics of Allometry. *Integrative and Comparative Biology*, 59, 1369–1381.
412 <https://doi.org/10.1093/icb/icz105>

413 Head, J.J., & Polly, P.D. (2015). Evolution of the snake body form reveals homoplasy in amniote
414 *Hox* gene function. *Nature*, 520, 86–89. <https://doi.org/10.1038/nature14042>

415 Jones, K.E. (2018). Regions. Find regions in serially-homologous structures. R package.
416 <https://github.com/katrinajones/regions>

417 Jones, K.E., Angielczyk, K.D., Polly, P.D., Head, J.J., Fernandez, V., Lungmuzz, J.K., Tulga, S.,
418 & Pierce, S.E. (2018). Fossils reveal the complex evolutionary history of the mammalian
419 regionalized spine. *Science*, 361, 1249–1252. . <https://doi.org/10.1126/science.aar3126>

420 Jones, K.E., Gonzalez, S., Angielczyk, K.D., & Pierce, S.E. (2020). Regionalization of the axial
421 skeleton predates functional adaptation in the forerunners of mammals. *Nature Ecology*
422 *and Evolution*, 4, 470–478. <https://doi.org/10.1038/s41559-020-1094-9>

423 Klingenberg, C.P. (2008). Morphological integration and developmental modularity. *Annual*
424 *Review of Ecology, Evolution and Systematics*, 39, 115–132.
425 <https://doi.org/10.1146/annurev.ecolsys.37.091305.110054>

426 Klingenberg, P. (2009). Morphometric integration and modularity in configurations of
427 landmarks: Tools for evaluating a-priori hypotheses. *Evolution and Development*, 11,
428 405–421. <https://doi.org/10.1111/j.1525-142X.2009.00347.x>

429 Klingenberg, C.P. (2011). MorphoJ: an integrated software package for geometric
430 morphometrics. *Molecular Ecology Resources*, 11, 353–357.
431 <https://doi.org/10.1111/j.1755-0998.2010.02924.x>

432 Klingenberg, C.P. (2013). Cranial integration and modularity: insights into evolution and
433 development from morphometric data. *Hystrix*, 24, 43–58.
434 <https://doi.org/10.4404/hystrix-24.1-6367>

435 Klingenberg, C.P., Barluenga, M., & Meyer, A. (2002). Shape analysis of symmetric structures:
436 quantifying variation among individuals and asymmetry. *Evolution*, 56, 1909–1920.

437 Krumlauf, R. (1994). *Hox* genes in vertebrate development. *Cell*, 78, 191–201.
438 <https://doi.org/10.1111/j.0014-3820.2002.tb00117.x>

439 Kuratani, S. (2009). Modularity, comparative embryology and evo-devo: Developmental
440 dissection of evolving body plans. *Developmental Biology*, 332, 61–69.
441 <https://doi.org/10.1016/j.ydbio.2009.05.564>

442 Lanza, B., Arntzen, J.W., & Gentile, E. (2010). Vertebral numbers in the Caudata of the Western
443 Palaearctic (Amphibia). *Atti del Museo Civico di Storia Naturale di Trieste*, 54, 3–114.

444 Litvinchuk, S.N., & Borkin, L.J. (2003). Variation in number of trunk vertebrae and in count of
445 costal grooves in salamanders of the family Hynobiidae. *Contributions to Zoology*, 72,
446 195–209. <https://doi.org/10.1163/18759866-07204001>

447 Lowie, A., De Kegel, B., Wilkinson, M., Measey, J., O'Reilly, J.C., Kley, N.J., Gaucher, P.,
448 Brecko, J., Kleinteich, T., Herrel, A. & Adriaens, D., (2022). Regional differences in
449 vertebral shape along the axial skeleton in caecilians (Amphibia: Gymnophiona). *Journal*
450 *of Anatomy*, 241, 716–728. <https://doi.org/10.1111/joa.13682>

451 Mallo, M., Wellik, D.M., & Deschamps, J. (2010). *Hox* genes and regional patterning of the
452 vertebrate body plan. *Developmental Biology*, 344, 7–15.
453 <https://doi.org/10.1016/j.ydbio.2010.04.024>

454 Manly, B.F.J. (2007). Randomization, bootstrap and Monte Carlo methods in biology. Boca
455 Raton: Chapman & Hall/CRC.

456 McCane, B., & Kean, M.R. (2011). Integration of parts in the facial skeleton and cervical
457 vertebrae. *American Journal of Orthodontics and Dentofacial Orthopedics*, 139, e13–
458 <https://doi.org/10.1016/j.ajodo.2010.06.016>

459 Mivart, G. (1870). On the axial skeleton of the Urodela. *Proceedings of the Zoological Society of*
460 *London*, 1870, 260–278.

461 Mitteroecker P., & Bookstein F.L. (2007). The conceptual and statistical relationship between
462 modularity and morphological integration. *Systematic Biology*, 56, 818–836.
463 <https://doi.org/10.1080/10635150701648029>

464 Neaux, D., Guy, F., Gilissen, E., Coudyzer, W., & Ducrocq, S. (2013). Covariation between
465 midline cranial base, lateral basicranium, and face in modern humans and chimpanzees: a
466 3D geometric morphometric analysis. *The Anatomical Record*, 296, 568–579.
467 <https://doi.org/10.1002/ar.22654>

468 Olson, E.C., & Miller, R. L. (1958). Morphological Integration. Chicago: University of Chicago
469 Press.

470 Pabijan, M., Zieliński, P., Dudek, K., Stuglik, M., & Babik, W. (2017). Isolation and gene flow
471 in a speciation continuum in newts. *Molecular Phylogenetics and Evolution*, 116, 1–12.
472 <https://doi.org/10.1016/j.ympev.2017.08.003>

473 R Core Team. (2021). R: A language and environment for statistical computing. R Foundation
474 for Statistical Computing, Vienna, Austria. <https://www.R-project.org/>.

475 Randau, M., & Goswami, A. (2017). Morphological modularity in the vertebral column of
476 Felidae (Mammalia, Carnivora). *BMC Evolutionary Biology*, 17, 133.
477 <https://doi.org/10.1186/s12862-017-0975-2>

478 Rohlf, F.J., & Slice, D.E. (1990). Extensions of the Procrustes method for the optimal
479 superimposition of landmarks. *Systematic Zoology*, 39, 40–59.
480 <https://doi.org/10.2307/2992207>

481 Rohlf, J., & Corti, M. (2000). Use of two-block partial least-squares to study covariation in
482 shape. *Systematic Biology*, 49, 740–753. <https://doi.org/10.1080/106351500750049806>

483 Sarkar, D. (2008). *Lattice: Multivariate Data Visualization with R*. New York: Springer.

484 Sarkar, D., & Andrews, F. (2019). *LatticeExtra: Extra graphical utilities based on Lattice*. R
485 package version 0.6-29. <https://CRAN.R-project.org/package=latticeExtra>

486 Scholtes, S.J., Arntzen, J.W., Ajduković, M., & Ivanović, A. (2021). Variation in vertebrae shape
487 across small-bodied newts reveals functional and developmental constraints acting upon
488 the trunk region. *Journal of Anatomy*, 240, 639–646. <https://doi.org/10.1111/joa.13591>

489 Shearman, R.M., & Burke, A.C. (2009). The lateral somitic frontier in ontogeny and phylogeny.
490 *Journal of Experimental Zoology Part B: Molecular and Developmental Evolution*, 312,
491 603–612. <https://doi.org/10.1002/jez.b.21246>.

492 Slijepčević, M., Galis, F., Arntzen, J.W. & Ivanović, A., (2015). Homeotic transformations and
493 number changes in the vertebral column of *Triturus* newts. *PeerJ*, 3, p.e1397.
494 <https://doi.org/10.7717/peerj.1397>

495 Toli, E.A., Bounas, A., Merilä, J., & Sotiropoulos, K. (2022). Genetic diversity and detection of
496 candidate loci associated with alternative morphotypes in a tailed amphibian. *Biological*
497 *Journal of the Linnean Society*, 137, 465–474. <https://doi.org/10.1093/biolinnean/blac103>

498 Urošević, A., Ajduković, M., Arntzen, J.W., & Ivanović, A. (2020). Morphological integration
499 and serial homology: a case study of the cranium and anterior vertebrae in salamanders.
500 *Journal of Zoological Systematics and Evolutionary Research*, 58, 1206–1219.
501 <https://doi.org/10.1111/jzs.12374>

502 Wagner, G.P., & Altenberg, L. (1996). Complex adaptations and the evolution of evolvability.
503 *Evolution*, 50, 967–976. <https://doi.org/10.1111/j.1558-5646.1996.tb02339.x>

504 Wainwright, P.C. (2007). Functional versus morphological diversity in macroevolution. *Annual*
505 *Review of Ecology, Evolution, and Systematics*, 38, 381–401.
506 <https://doi.org/10.1146/annurev.ecolsys.38.091206.095706>

507 Wellik, D.M. (2007). *Hox* patterning of the vertebrate axial skeleton. *Developmental Dynamics*,
508 236, 2454–2463. <https://doi.org/10.1002/dvdy.21286>

509 Worthington, R.D., & Wake, B.D. (1972). Patterns of regional variation in the vertebral column
510 of terrestrial salamanders. *Journal of Morphology*, 137, 257–277. .
511 <https://doi.org/10.1002/jmor.1051370302>

512 Young, N.M., & Hallgrímsson, B. (2005). Serial homology and the evolution of mammalian
513 limb covariation structure. *Evolution*, 59, 2691–2704. [https://doi.org/10.1111/j.0014-](https://doi.org/10.1111/j.0014-3820.2005.tb00980.x)
514 [3820.2005.tb00980.x](https://doi.org/10.1111/j.0014-3820.2005.tb00980.x)

515 Zelditch M.L., Swiderski D.L., & Sheets D.H. (2012). Geometric morphometrics for biologists: a
516 primer. San Diego: Elsevier Academic Press.

517 Zelditch M.L., & Goswami A. (2021). What does modularity mean? *Evolution & Development*,
518 23, 377–403. <https://doi.org/10.1111/ede.12390>

519

520 **Tables**

521

522 **Table 1.** Concepts of regional differentiation of the presacral vertebral column in tailed
523 amphibians.

Concept	Traditional, one region
Regions recognized	Trunk
Source	Mivart (1870), Duelman & Trueb (1994), Slijepčević et al. (2015)

Concept	A three-regions pattern conserved across the Tetrapods
Regions recognized	Cervical, anterior dorsal and posterior dorsal
Source	Jones et al. (2018)

Concept	A two-regions pattern based on morphological disparity and functional differentiation
Regions recognized	Anterior trunk and posterior trunk
Source	Worthington & Wake (1972), Govedarica et al. (2017), Scholtes, et al. (2021), present study

524

525

526

527

528

529

530

531

532

533

534 **Table 2.** Homogeneity of slopes in *Lissotriton v. vulgaris*, with the effect of vertebrae, size
 535 (logCS) and vertebra \times logCS interaction, tested by a multivariate analysis of covariance.
 536 Statistically significant interaction indicates heterogenous regression slopes.

Effect	Wilks' Lambda	F	Effect df	Error df	P
Vertebra	0.836	1.74	55	2429.06	0.0007
LogCS	0.524	95.26	5	524.00	<0.0001
Vertebra \times logCS	0.837	1.73	55	2429.06	0.0008

537
 538
 539
 540
 541
 542
 543
 544
 545
 546
 547
 548
 549
 550
 551
 552

553 **Table 3.** Results of MANCOVA tests for differences in allometric slopes among vertebrae.
 554 Vertebrae are numbered from 1 to 12. Wilk's lambda values in boldface type denote statistical
 555 significance for pairwise comparisons at $P < 0.05$ after Bonferroni correction, with an adjusted
 556 alpha value of 0.0008.

	1	2	3	4	5	6	7	8	9	10	11
2	0.892										
3	0.852	0.981									
4	0.845	0.915	0.865								
5	0.828	0.829	0.713	0.961							
6	0.906	0.888	0.842	0.931	0.932						
7	0.871	0.899	0.803	0.968	0.965	0.949					
8	0.846	0.966	0.953	0.936	0.833	0.919	0.868				
9	0.910	0.933	0.892	0.961	0.960	0.975	0.974	0.952			
10	0.928	0.984	0.944	0.925	0.841	0.927	0.904	0.954	0.951		
11	0.874	0.975	0.957	0.963	0.869	0.912	0.888	0.984	0.946	0.966	
12	0.873	0.933	0.883	0.848	0.798	0.775	0.808	0.875	0.836	0.925	0.907

557

558

559

560

561

562

563

564

565

566

567 **Table 4.** Results of a segmented linear regression analysis on vertebrae shape averaged for
 568 *Lissotriton* (sub)species. The most likely regionalization models are shown in boldface type.
 569

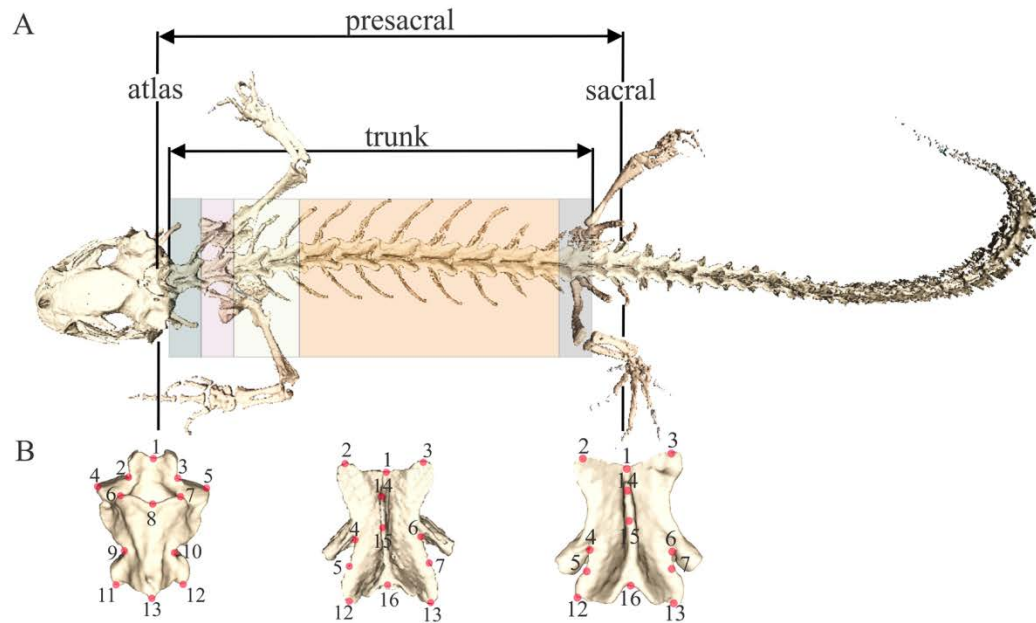
(Sub)species	Regions	T1	T2	sumRSS	AICc	deltaAIC	model_lik	Ak_weight
<i>Lissotriton schmidtleri</i>	2	5	0	2.75	- 21.19	0.00	1.0000	0.9937
	3	3	5	0.68	- 10.92	10.26	0.0059	0.0059
	1	0	0	12.35	-5.85	15.34	0.0005	0.0005
<i>Lissotriton v. ampelensis</i>	2	5	0	3.02	- 18.86	0.00	1.0000	0.8253
	3	4	7	0.55	- 15.74	3.12	0.2102	0.1735
	1	0	0	12.35	-5.84	13.03	0.0015	0.0012
<i>Lissotriton v. meridionalis</i>	2	5	0	2.28	- 25.61	0.00	1.0000	0.9998
	3	3	9	0.78	-7.71	17.90	0.0001	0.0001
	1	0	0	11.91	-6.71	18.89	0.0001	0.0001
<i>Lissotriton v. vulgaris</i>	2	5	0	1.81	- 40.06	0.00	1.0000	0.9654
	3	4	9	0.56	- 33.40	6.66	0.0359	0.0346
	1	0	0	12.99	-8.14	31.93	0.0000	0.0000

571 **Figures**

572

573

574



575

576 **Figure 1.** Morphological differentiation and regionalization of the presacral vertebral column in
577 *Lissotriton* newts showing (A) different morphologies of trunk vertebrae, indicated by different
578 color shadings, and (B) the configuration of the landmarks used to describe the shape of the atlas
579 and the trunk and sacral vertebrae.

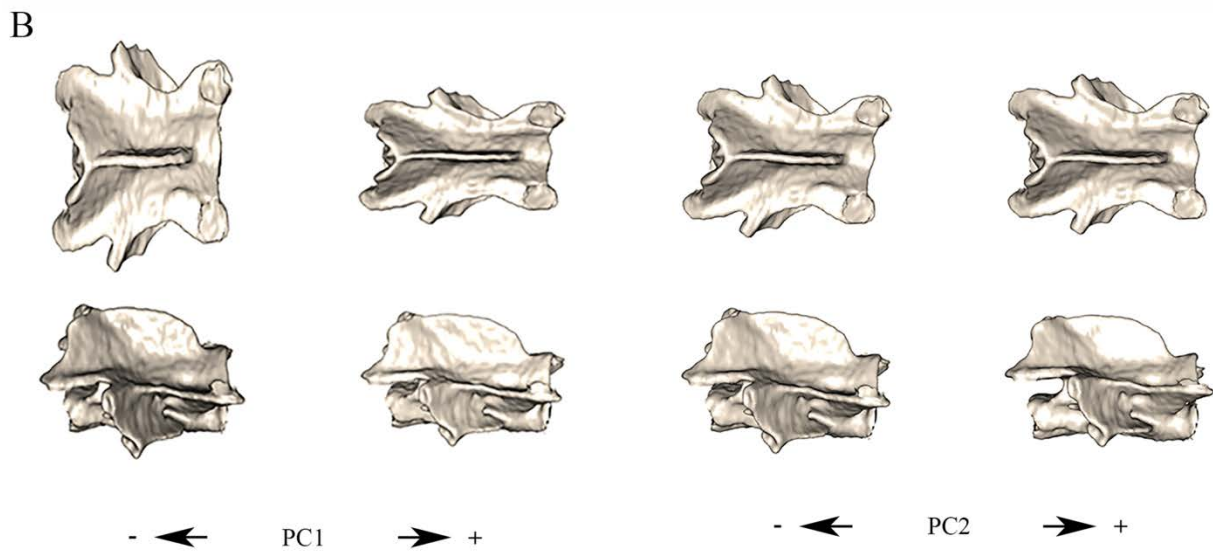
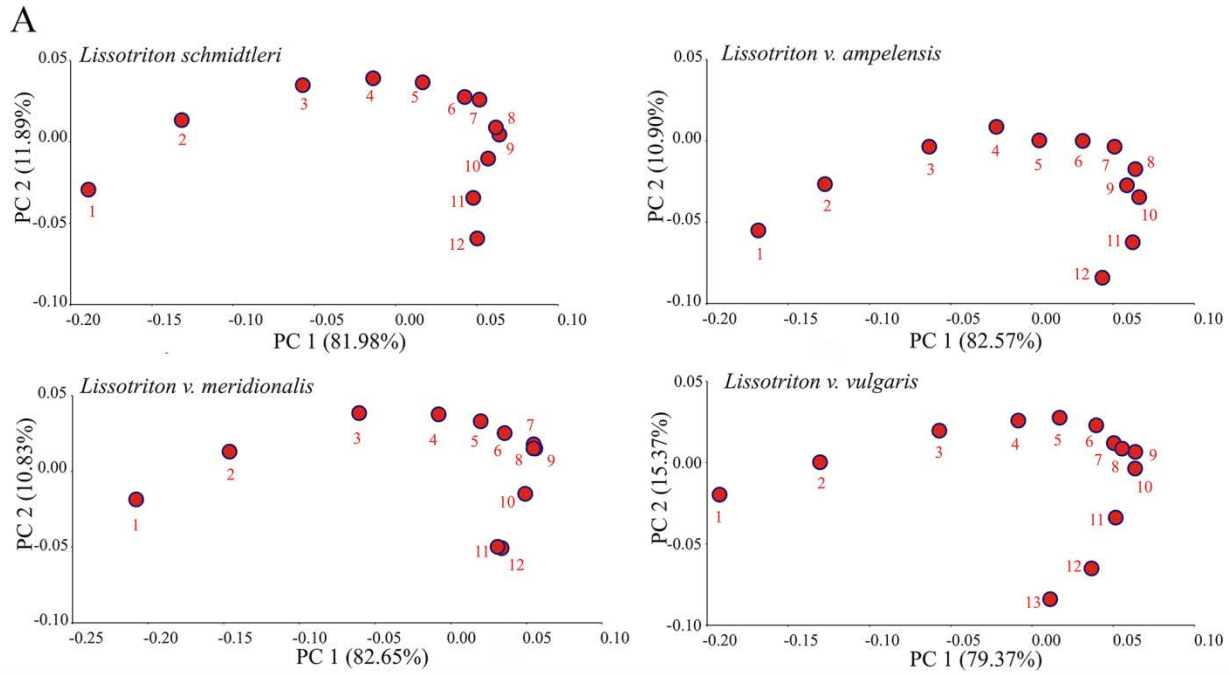
580

581

582

583

584



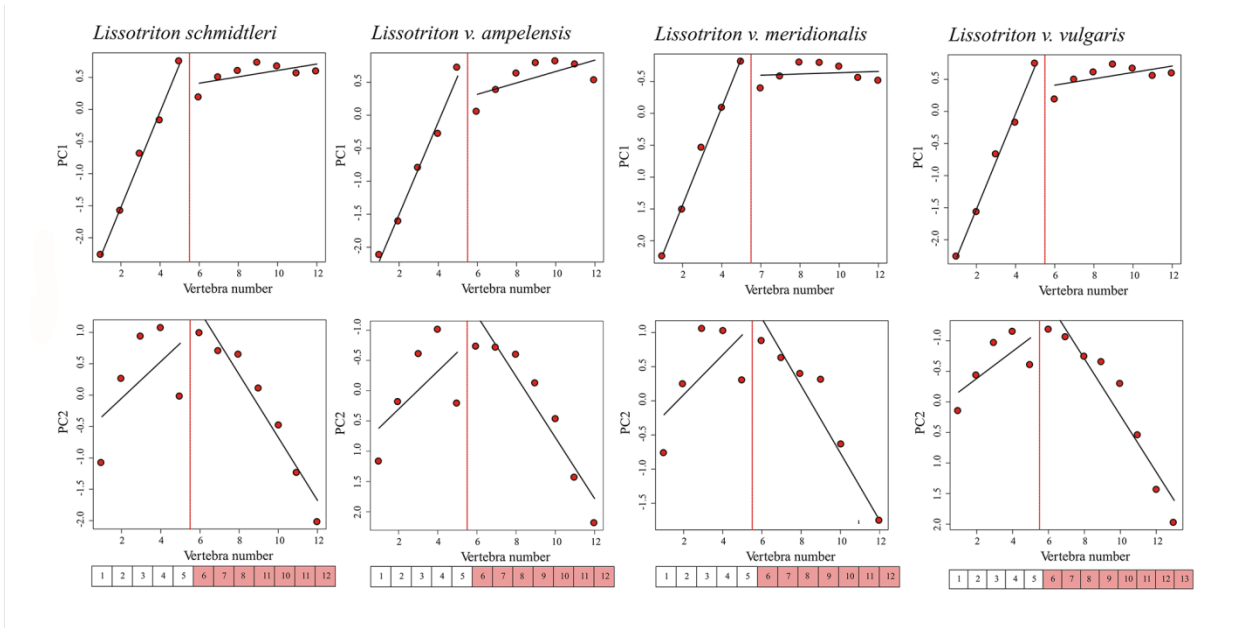
585

586

587 **Figure 2.** Shape changes of trunk vertebrae in four *Lissotriton* taxa with (A) the position of the
 588 trunk vertebrae over numbers 1 to 12 or 13, and (B) the gradient of shape changes over the first
 589 and second principal component axis.

590

591
592
593
594
595



596
597
598
599
600
601
602
603
604
605

Figure 3. Results of segmented linear regression analysis of the trunk vertebrae in four *Lissotriton* taxa. Dots show the scores along the first (top panel) and second (bottom panel) axis of a principal component analysis for vertebrae 1-12. Region models are shown in bars below each of the graphs.

606

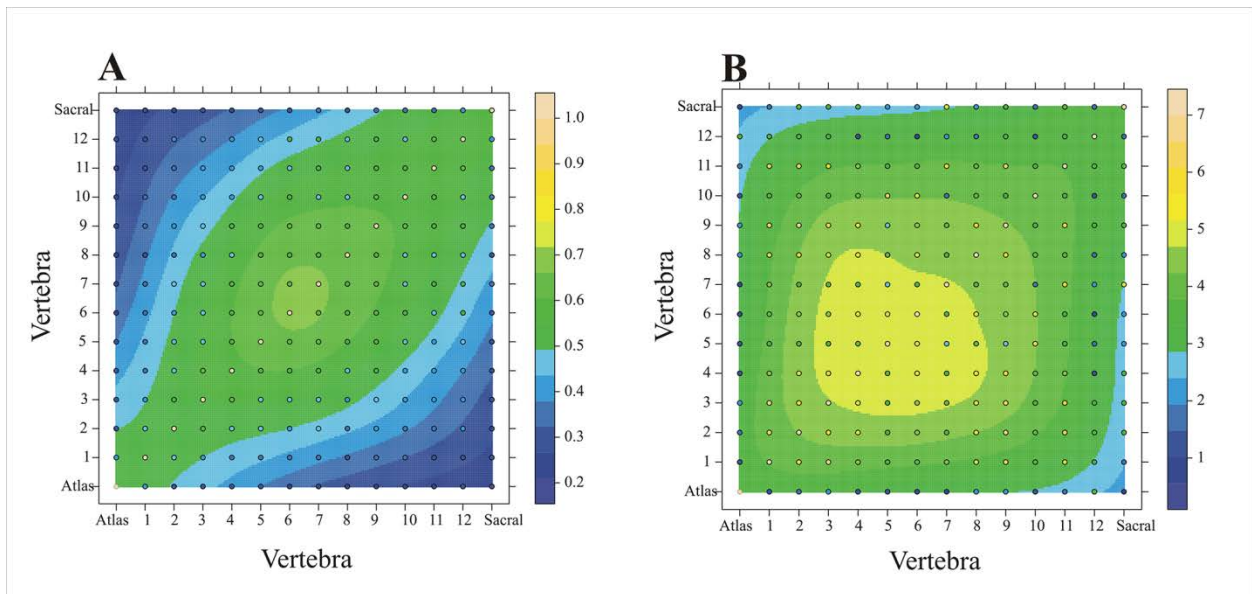
607

608

609

610

611



612

613 **Figure 4.** Heat maps presenting patterns of morphological integration of the presacral vertebral
614 column in *Lissotriton* newts. Dots represent individual pairwise correlations corrected for
615 (sub)species for (A) RV scores on the symmetric component of the shape variation, and (B) z-
616 scores on total shape. For actual values see color bars.

617

618 **Appendices**

619

620 **Appendix I.** Analyzed material with scientific name, taxonomic authority, sample size (N),
 621 collection identification numbers (ID), locality of origin and type of preservation (ethanol
 622 preserved whole animals and glycerin stored skeletons).

623

Species and (sub)species	N	Collection	ID	Locality	Preservation
<i>Lissotriton schmidleri</i> (Raxworthy, 1988)	13	IBISS	OZ 58 G21921; OZ 58 G21932; OZ 58 G21934; OZ 58 G2193235; OZ 58 G21937-40; OZ 58 G21948-50; OZ 58 G21952; OZ 58 G21953	Efes, Turkey	Glycerin
<i>L. v. meridionalis</i> (Boulenger, 1882)	8	IBISS	2373 15625; 2373 15629; 2373 15633; 2373 15641- 44; 2373 15646	Podstrmec, Slovenia	Ethanol
<i>L. v. ampelensis</i> (Fuhn,1951)	6	IBISS	OZ 62 G22595; OZ 62 G22598; OZ 62 G22600- 03	Garda de Sus, Romania	Glycerin
<i>L. v. vulgaris</i> (Linnaeus, 1758)	5	IBISS	2579 17780; 2579 17788; 2579 17795; 2579 17797; 2579 17813	Valjevo, Serbia	Glycerin
<i>L. v. vulgaris</i> (Linnaeus, 1758)	20	ZMA.RENA	9270 (1-20)	Marcillé-la- Ville, France	Ethanol
<i>L. v. vulgaris</i> (Linnaeus, 1758)	22	RMNH.RENA	9521 (1-14); (G, H, J-M, O, P)	Hoensbroek, The Netherlands	Ethanol

624 IBISS – University of Belgrade, Institute for Biological Research “Siniša Stanković” – National Institute of the
 625 Republic of Serbia, RMNH.RENA and ZMA.RENA – Naturalis Biodiversity Center, Leiden, The Netherlands.

626

627 **Appendix II.** The configuration of 14 three-dimensional landmarks identified on the atlas and 18
 628 three-dimensional landmarks on the trunk and sacral vertebrae of *Lissotriton* newts. For a
 629 visualization see Figure 1B.

630

Structures	Number	Description
Atlas	1	Tip of processus odontoideus
	2,3	Maximal constriction of processus odontoideus
	4,5	Most lateral point of occipital joint
	6,7	Tip of the lamina
	8	Tip of the vertebra on the dorsal side
	9,10	Maximal constriction of vertebra
	11,12	Maximal curvature of the postzygapophysis
	13	The end of vertebra on the dorsal side
	14	Tip of the cotylus
Trunk and sacral vertebrae	1	Neural arch – anterior, above vertebral foramen
	2,3	Prezygapophysae – antero-lateral margins
	4,6	Neural arch – lateral margin at the level of rib-bearers
	5,7	Maximal constriction of the postzygapophysis
	8,10	Parapophysae – articulation point
	9,11	Diapophysae – articulation point
	12,13	Postzygapophysae – posterio-lateral margins
	14	Neural spine – the most anterior part
	15	Neural spine – the middle part
	16	Neural spine – the most posterior part
17	The anterior tip of the condylus	
18	Tip of the cotylus	

631

632

633 **Supporting information**

634

635 **Supplementary data S1.** Raw morphometric data and Centroid Size values for the atlas, 1st to
636 12th (or 13th) trunk and sacral vertebra of *Lissotriton* (sub)species. Information is given on the
637 individual (ID), the (sub)species (Taxon) and the raw coordinates for altogether 32 landmarks
638 (RawCoord1 - RawCoord42 for atlas) or (RawCoord1 - RawCoord54 for trunk and sacral
639 vertebrae).

640

641 **Supplementary file S2.** R scripts used in the study for the packages *Regions* (Jones, 2018),
642 *Geomorph* (Adams et al., 2021), *Lattice* (Sarkar, 2008) and *Lattice Extra* (Sarkar & Andrews,
643 2019).

644

645 **Supplementary table S3.** Homogeneity of slopes for vertebrae allometry, with the effect of
646 (sub)species, size (logCS) and (sub)species x logCS interaction, tested by multivariate analysis
647 of covariance. Statistically significant (sub)species x logCS interactions indicate heterogenous
648 regression slopes. The Bonferroni adjusted alpha 0.05 value is 0.0036. Comparisons that are
649 statistically significant are in boldface type.

650

651 **Supplementary table S4.** Generalized Pearson correlation coefficients among vertebrae in
652 *Lissotriton* newts with RV values in the top panel and z-score in the bottom panel. The
653 Bonferroni adjusted value for alpha 0.05 is 0.00055. Data in boldface statistical significance of
654 the pairwise comparisons.